Efficient Solution-Processed Nanoplatelet-Based Light-Emitting Diodes with High Operational Stability in Air

Umberto Giovanella*, Mariacecilia Pasini, Monica Lorenzon, Francesco Galeotti, Claudio Lucchi, Francesco Meinardi, Silvia Luzzati, Benoit Dubertret*, and Sergio Brovelli*

Abstract

Colloidal nanoplatelets (NPLs), owing to their efficient and narrow-band luminescence, are considered as promising candidates for solution-processable light-emitting diodes (LEDs) with ultrahigh color purity. To date, however, the record efficiencies of NPL-LEDs are significantly lower than those of more-investigated devices based on spherical nanocrystals. This is particularly true for red-emitting NPL-LEDs, the best-reported external quantum efficiency (EQE) of which is limited to 0.63% (EQE = 5% for green NPL-LEDs). Here, we address this issue by introducing a charge-regulating layer of a polar and polyelectrolytic polymer specifically engineered with complementary trimethylammonium and phosphonate functionalities that provide high solubility in orthogonal polar media with respect to the NPL active layer, compatibility with the metal cathode, and the ability to control electron injection through the formation of a polarized interface under bias. Through this synergic approach, we achieve EQE = 5.73% at 658 nm (color saturation 98%) in completely solution processed LEDs. Remarkably, exposure to air increases the EQE to 8.39%, exceeding the best reports of red NPL-LEDs by over 1 order of magnitude and setting a new global record for quantum-dot LEDs of any color embedding solution-deposited organic interlayers. Considering the emission quantum yield of the NPLs (40 ± 5%), this value corresponds to a near-unity internal quantum efficiency. Notably, our devices show exceptional operational stability for over 5 h of continuous drive in air with no encapsulation, thus confirming the potential of NPLs for efficient, high-stability, saturated LEDs.

KEYWORDS:Nanocrystal quantum dots nanoplatelets CdSe CdS polar polymer light-emitting diodes charge-injecting layers

Since their introduction in 2008, (1) colloidal semiconductor nanoplatelets (NPLs) have become the subject of intense research efforts (2−4) because they uniquely combine the processing advantages of solution-based materials with the physical properties of two-dimensional quantum wells, (3,5−10) including tunable luminescence controlled by the particle thickness, (2,3,7,11−14) high emission efficiency, (15) strong exciton and biexciton binding energy, (3,11,16,17) and suppressed Auger recombination. (10,18,19) These features render NPLs promising candidates in several optoelectronic and photonic technologies, such as lasers, (10,17,20,21) photodetectors, (22,23) phototransistors, (24−26) sensors, (27) and light-emitting diodes (LEDs). (12,28−30) In this latter application, the spectrally narrow electroluminescence of NPLs, (28) resulting from the highly homogeneous particle thickness unaffected by Oswald ripening (31) and easily achievable in scaled-up quantities, offers an important advantage over spherical colloidal quantum dots (QDs), which require strict control over the three dimensions with regard to their size, morphology, and surface chemistry for obtaining monodispersed ensembles of well-passivated particles. Despite this promise, LEDs based on NPLs have been investigated much less than their spherical counterparts, (32) and their record performance is, therefore, still lower than that of state-of-the-art QD-LEDs. (33,34) To date, the highest external quantum efficiency (EQE) of NPL-LEDs was reported by Zhang et al., who achieved EQE = 5% using green-emitting NPLs, (12) whereas the best performance in the red spectral region can be traced back to the first demonstration of NPL-LEDs by Chen et al., (28) who achieved EQE = 0.63% using core–shell CdSe/CdZnS NPLs. In comparison, red LEDs incorporating QDs with near-unity luminescence efficiency have been obtained with EQEs as high as 18–20%, (29,30) corresponding to ∼100% internal quantum efficiency.

The improvement of the performances of red NPL-LEDs is, therefore, a particularly relevant task in this field.

Here, we aim to address this problem by applying an improved version of a recently introduced strategy for producing highly efficient QD-LEDs exclusively through solution-based processes. (35) Specifically, our approach uses conjugated polymers with polar and electrolytic side-chains (also referred to as conjugated polyelectrolytes or CPEs) as electron-transport materials to maximize carrier balance in the device and improve the compatibility with the metal cathode. The distinctive characteristic of CPEs is the functionalization of their conjugated backbone with polar (36−39) or ionic substitutes (40−42) (in either a cationic, anionic, or zwitterionic form) (43) that renders the polymer easily soluble in polar solvents (i.e., methanol or water), (40,41,44) which are orthogonal to the nonpolar media typically used for processing the active layer in QD- and NPL-LEDs. This enables one to deposit the electron-transport layer (ETL) using wet methods (i.e., spin-coating and roll-to-roll or inkjet printing) without damaging the underlying active layer. (45−49) In addition to this, using CPEs as ETLs enables us to tune the electron-injection barrier between the metallic cathode and the active QD layer (39,47,35) by the creation of interface dipoles due to the alignment of the polar and ionic functionalities to the applied electric field, (50,51) resulting in improved carrier balance (41,48−50) and higher EQEs. (38,40,52,41)

The benefits of CPEs have mostly been exploited in organic LEDs (41,43,44,53) and solar cells, (52,54,55) whereas their application to QD-based devices is still limited. By using polar and electrolytic polymers as an electron-transport and hole-blocking layer, we recently fabricated solution-processed QD-LEDs with EQEs as high as 6.1% (ref (35)), corresponding to a ∼200% enhancement with respect to previous reports on QD-LEDs in direct architecture (56) employing solution-processed (57−59) or thermally evaporated organic interlayers. (56,60−62) In these devices, the CPE layer acted as electrically tunable electron barrier that dramatically improved the charge balance by partially reducing the electron current through the junction so as to match the minority hole population injected by the anode into the deep valence band of CdSe. Along the same line, Cho et al. (63) used poly(amidoamine) dendrimers in inverted-structure QD-LEDs to control the charge injection from the ITO cathode and to graft the QDs to the underlying ZnO nanoparticles ETL, obtaining EQE = 11.36%. To date, polar and electrolytic ETLs have never been applied to NPL-LEDs. Taking inspiration from these studies, for this work, we expressly designed a multifunctional copolymer featuring alternate fluorene moieties with two long side-chains terminated with either a trimethylammonium cation (TMA, with a Br– counter-anion) or a phosphonate group (Figure 1a).

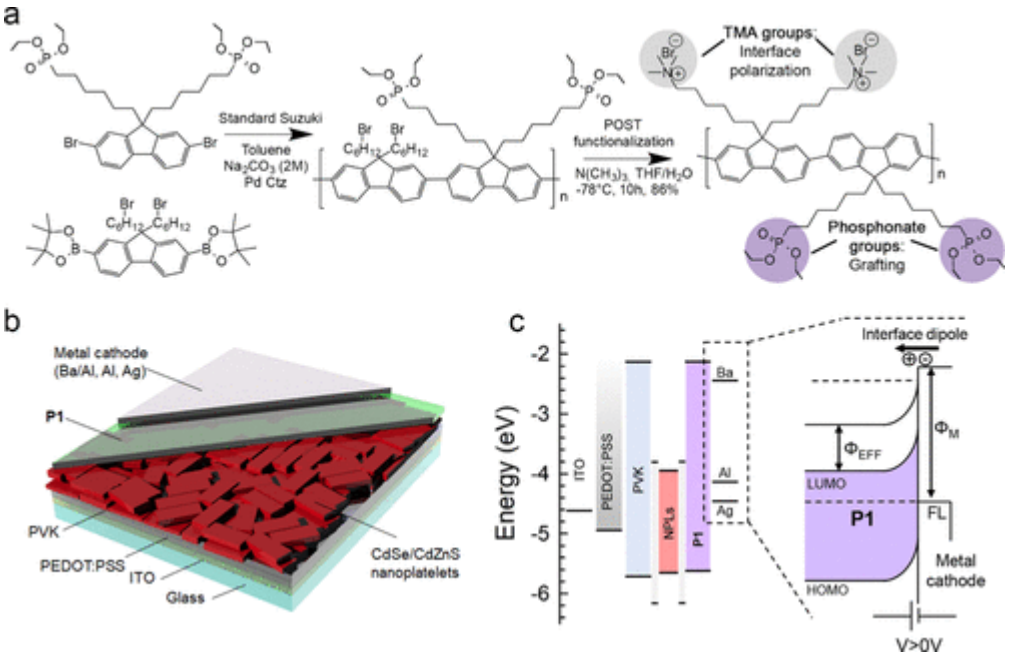

Figure 1. (a) Synthesis of alcohol-soluble polyfluorene derivative used as ETL in all-solution-processed NPL-LEDs, namely poly[(2,7-(9,9′-bis(6′-diethoxylphosphorylhexyl)-fluorene)-alt-(2,7-(9,9′-bis(6″-trimethylammonium bromide)hexyl)-fluorene)]] (P1) starting from the intermediates 2,7-bis-[9,9′-bis(6″-bromohexyl)fluorenyl]-4,4,5,5-tetramethyl [1.3.2]dioxa-borolane (1) and 2,7-dibromo-9,9-bis(6′-diethoxylphosphorylhexyl)-fluorene (2). (b) Multilayered-device architecture for the NPL-LEDs: ITO/PEDOT:PSS/PVK/NPLs/P1/metal cathode. (c) Flat-band energy level diagram of the device (with respect to the vacuum level). The dashed rectangle highlights the metal–polymer interface, which is magnified in the right panel, showing the band-bending effect originating from the metal–polymer contact and the downward energy shift caused by the interface dipole under the application of direct bias.

The TMA functionality serves the purpose of creating the interface dipole under an applied bias that controls the injection of electrons in the active layer. The phosphonate group, however, has the particular capability of effectively grafting the polymeric layer onto the aluminum cathode by the formation of P–O–Al coordination at the metal–organic interface during the top deposition of Al atoms. Altogether, the CPE interlayer improves the device performances by assisting carrier crossing through the interface, (64,65) by lowering the cathode work function, (64,65) and by suppressing nonradiative exciton dissociation at the cathodic interface. (65) Through this approach, in combination with CdSe/CdZnS NPLs, we obtain all-solution-based NPL-LEDs with nearly perfectly saturated 658 nm electroluminescence (saturation of 98%) and EQE = 5.73%, which matches the best performances of green emitting NPL-LEDs and corresponds to an enhancement of 1 order of magnitude with respect to previous reports in the red spectral region. In contrast to expectations, exposing our devices to ambient air (50% humidity) has a strong beneficial effect on their efficiency, resulting in a record EQE of 8.39% after 5.5 h of air exposure. This is particularly remarkable considering that the photoluminescence (PL) quantum yield of the employed NPLs is ΦPL = 40 ± 5%. The use of optimized NPLs with a unity emission yield indicates that a projected EQE as high as ∼21% could be achieved, corresponding to the maximum efficiency of ideal planar LEDs without engineered light out-coupling. (66,67) Finally, stress-test measurements show no efficiency drop, even after over 4 h of continuous operation in humid air (50%) with no device encapsulation, demonstrating the remarkable operational stability of the NPL-LEDs.

Results and Discussion

The CdSe/CdZnS core–shell NPLs with a 4 monolayer (ML) thick CdSe core coated on each side with 3 nm of CdZnS shell were obtained from Nexdot and synthesized according to the route described in the Supporting Information. The functionalized copolymer poly[(2,7-(9,9′-bis(6′-diethoxylphosphorylhexyl)-fluorene)-alt-(2,7-(9,9′-bis(6″-trimethylammonium bromide)hexyl)-fluorene))] (P1) was synthesized according to the procedure described in Figure 1a and explained in detail in the Supporting Information. The CdSe/CdZnS NPLs and P1 were incorporated into LEDs in direct architecture as schematically depicted in Figure 1b. The devices were fabricated by successive spin-coating of the charge transport and active layers onto a glass substrate coated with patterned indium tin oxide (ITO), a poly(3,4-ethylenedioxythiophene) polystyrenesulfonate (PEDOT:PSS, 50 nm) hole-injecting layer and a polyvinyl carbazole (PVK, 30 nm) hole-transport layer (HTL) that further constrains the electrons injected from a metal cathode (120 nm Al, 4 nm Ba, and 120 nm Al or 120 nm Ag) inside the NPL active layer. The NPL film (65 nm) was deposited from a hexane solution (30 mg/mL) and covered with a ∼15–20 nm ETL of P1 spin-coated from ethanol (5 mg/mL). The adoption of orthogonal solvents for NPLs and P1 enables their consecutive deposition with no measurable damage to the NPLs active layer, as demonstrated by the device performances reported later. The flat-band energy diagram of the device layers with respect to vacuum is shown in Figure 1c. The frontier levels of P1 are EHOMO ≈ −5.7 eV for the highest occupied molecular orbital and ELUMO ≈ −2.2 eV for the lowest unoccupied molecular orbital, consistent with the typical values for polyfluorene derivatives and indicating that the functionalization with the phosphonate and the trimethylammonium side groups

does not affect the electronic structure of the conjugated backbone. (35,68,69)Figure 1c reports a schematic depiction of the interface between P1 and a representative metal cathode: under direct bias, ion migration and molecular reorientation lead to the formation of an interface dipole directed from the metal surface to the polymeric layer, causing a polarization-induced downward shift of the vacuum level and of the LUMO level of P1. Such an energy shift leads to a drop in the polymer work function (ΦP1) to an "effective" ΦEFFP1 value and to the narrowing of the electron injection barrier. (43,70) Through this mechanism, the P1 interlayer tunes electron injection into the NPL active layer, improving the electron–hole balance and LED efficiency. The optical absorption and PL spectra of P1 are reported in Figure 2a, showing a close resemblance to the spectral profiles of bare poly(dioctylfluorene), with a low-energy absorption band at ∼390 nm (35,71,72) and a structured PL band with first vibronic peak at 425 nm, thus confirming that the electronic properties of the polymer backbone are unaffected by the side-chains. The optical absorption peak at 344 nm and PL spectra of PVK are also reported showing the characteristic broad emission at ∼420 nm. No emission from P1 or PVK is observed in the electroluminescence (EL) spectra of the NPL-LEDs reported later in this work, indicating that radiative exciton recombination takes place exclusively in the NPL active layer.

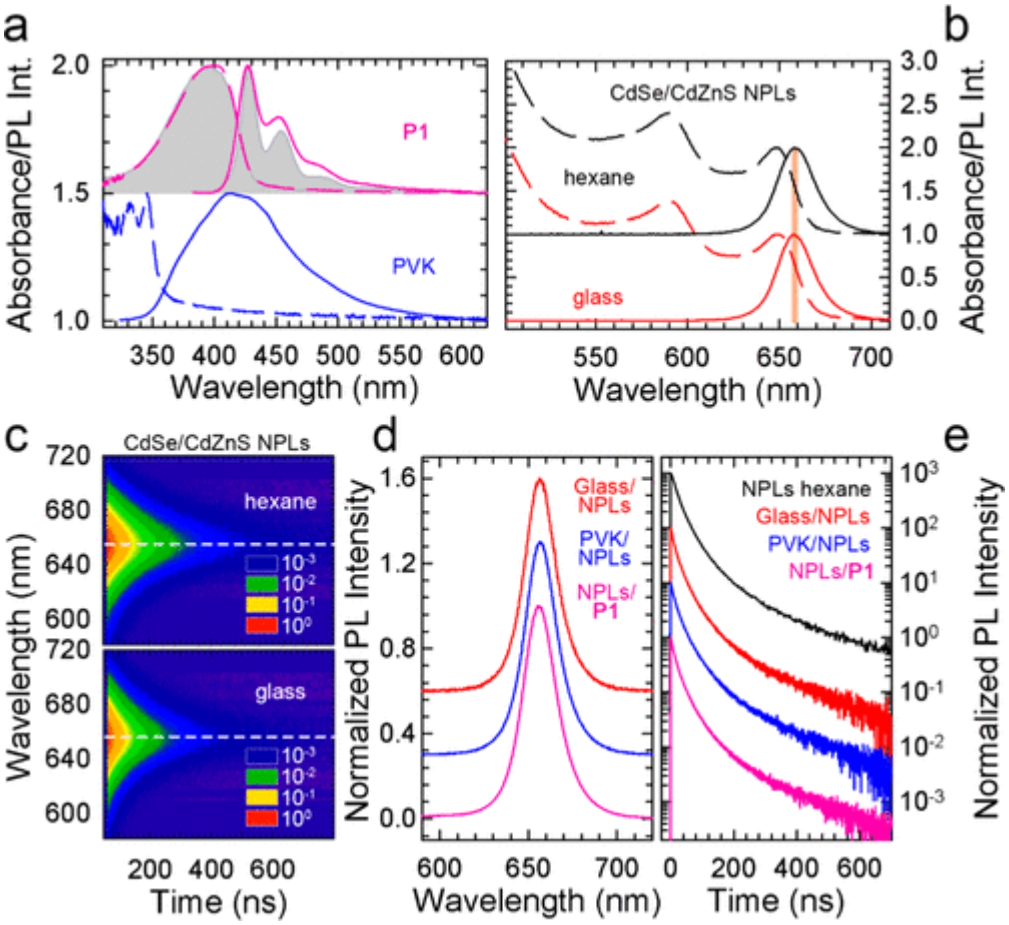

Figure 2. (a) Optical absorption (dashed lines) and normalized PL (solid lines, excitation at 340 nm) spectra of thin films of the polar polymer P1 (purple lines) and polyvinyl carbazole (PVK, blue lines). The absorption and PL spectra of poly (dioctylfluorene) are shown as gray shading for direct comparison to the functionalized P1 polymer. (b) Optical absorption (dashed lines) and normalized PL (solid lines) spectra of a dilute hexane solution of CdSe/CdZnS NPLs (black lines) and a film of the same NPLs deposited onto a glass substrate (red lines). (c) Contour plots of the PL time decay for a dilute hexane solution (top panel) and a film of CdSe/CdZnS NPLs on glass (bottom panel). The dashed white line is a guide for the eye to emphasize

the invariance of the PL peak position over time. (d) PL spectra and (e) decay curves of CdSe/CdZnS NPLs deposited onto different substrates, namely glass (red line), PVK (blue line), and P1 (purple line). The decay trace for a dilute hexane solution of CdSe/CdZnS NPLs is shown as a solid black line in panel e for direct comparison with the film dynamics. The spectra and PL decay curves are vertically shifted for clarity. All PL measurements on the NPLs are carried out at room temperature under pulsed 400 nm excitation with a power density of 40 nJ/cm2.

Because of their extended planar geometry, (73) NPLs have been observed to self-assemble into stacked lamellar structures, (74−76) leading, in solid samples, to spectral migration due to efficient interparticle energy transfer. (77−79) To test this effect, which could lower the color purity of the LEDs, prior to producing the devices, we measured the absorption and PL spectra of the CdSe/CdZnS NPLs dispersed in hexane and spin-cast onto a glass substrate (Figure 2b). The absorption profiles of the solution and of the film (65 nm) are essentially identical, with both showing the characteristic narrow peaks (3,16,27) associated with the optical transition of heavy and light holes, respectively, at 650 and 590 nm. The respective PL spectra are also perfectly superimposed to each other, with an emission maximum at ∼658 nm, indicating that spectral migration effects in the NPL film are negligible. This is confirmed by the contour plots of the PL decay reported in Figure 2c and by the normalized PL spectra measured at increasing delay time after the excitation pulse (Figures S1 and S2), showing no spectral shift over time in either system. Detailed analysis of the spectrally resolved PL decay traces shows identical decay curves across the emission profile in solution and a minor difference, close to our experimental resolution, in the NPL film. This points to the absence of energy-transfer processes between NPLs in solution and to essentially negligible effects in the film, likely due to the wide band gap in the alloyed CdZnS shell, similar to what was observed for CdSe/CdS hetero-QDs (80) and to the rapid film deposition by spin-coating. A furthermore relevant aspect to be considered when using polymeric interlayers and, in particular, CPEs with ionic side groups is the possible quenching effect on the emission efficiency of the active layer by charge-transfer processes. In QD-LEDs, this effect has been shown to lead to the charging of the QDs, (30,53) resulting in efficiency losses due to nonradiative Auger recombination. (81−84) To test this effect in our NPL-LEDs, we measured the PL spectrum, quantum efficiency, and decay dynamics of the NPL deposited on glass, P1, or PVK side-by-side. In all cases, the NPLs were excited through the substrate so as to primarily sample the particles in direct contact with the polymer interlayers. The PL quantum-yield measurements using an integrating sphere yield a constant QYPL = 40 ± 5% for all substrates. Accordingly, the PL dynamics and spectral profiles are essentially identical in all systems, thus excluding quenching effects by the organic interlayers (Figure 2d,e).

In light of the above considerations, we fabricated and tested NPL-LEDs in direct architecture (namely, ITO/PEDOT:PSS/PVK/NPLs/P1/metal cathode) as well as the reference devices without the P1 ETL following the procedure described above. The devices were assembled in a nitrogen atmosphere using water, chlorobenzene, hexane, and ethanol as the solvents for PEDOT:PSS, PVK, CdSe/CdZnS NPLs, and P1, respectively. For the metal cathode, we used aluminum, silver, or barium coated with an Al protective layer to test the effect of the metal work function on the device behavior.

Figure 3a reports the current density–voltage–luminance (J–V–L) response for two representative LEDs with and without the CPE interlayer and featuring an Al cathode. According to previous reports, the turn-on voltage (VON, measured as the voltage at which the luminance is 0.1 cd/m2; see the inset of Figure 3a) is found to be slightly lower for the LED containing the P1 ETL (4.05 V versus 4.5 V), which was ascribed to favored electron injection caused by the dipole-induced lowering of the cathode work function. (35,40,41,44,85−87) A similar reduction of the VON by the P1 interlayer is observed for NPL-LEDs with Ba and Ag electrodes, as reported in Figures S3 and S4. In addition to showing a systematically lower VON, the NPL-LEDs incorporating the P1 ETL exhibit significantly higher EQEs and brightness than the control devices,

reaching EQE = 5.73% and 1540 cd/m2 luminance, with respect to EQE = 2.47% and 891 cd/m2 (see Table 1 for the whole set of devices). Notably, all of our NPL-LEDs are significantly more efficient than the best-reported red-emitting NPL-LEDs (EQE = 0.63%), (28) with the devices containing the P1 interlayer showing a 5- to 10-fold improvement over the literature value. In agreement with carrier imbalance due to excessive electron population being a strong limiting factor for the performances of LEDs embedding CdSe/CdS nanostructures, the EQE of control devices (without P1) increases with increasing potential barrier for electron injection from the metal cathode (ΦBa < ΦAl < ΦAg; see the Figure 3b inset). Among our device set, the best performances are systematically exhibited by LEDs with both P1 and Al cathode, which is likely the combined result of the ability of the phosphonate functionality of P1 to graft onto aluminum and of the intermediate work function of the latter with respect to Ag and Ba, which renders the tunable potential barrier due to the interfacial polarization of the TMA side groups particularly effective in reducing excessive electron current into the active layer, leading to optimal carrier balance. Because of such a combination of effects, the trend of the EQE versus the electrode work function is not conserved in LEDs with a P1 interlayer. Notably, no electrical conditioning, observed earlier for QD-LEDs integrating CPE interlayers, is observed in our NPL-LEDs, which is likely due to the functionalization of P1 with TMA units that were absent in previous studies. (35)

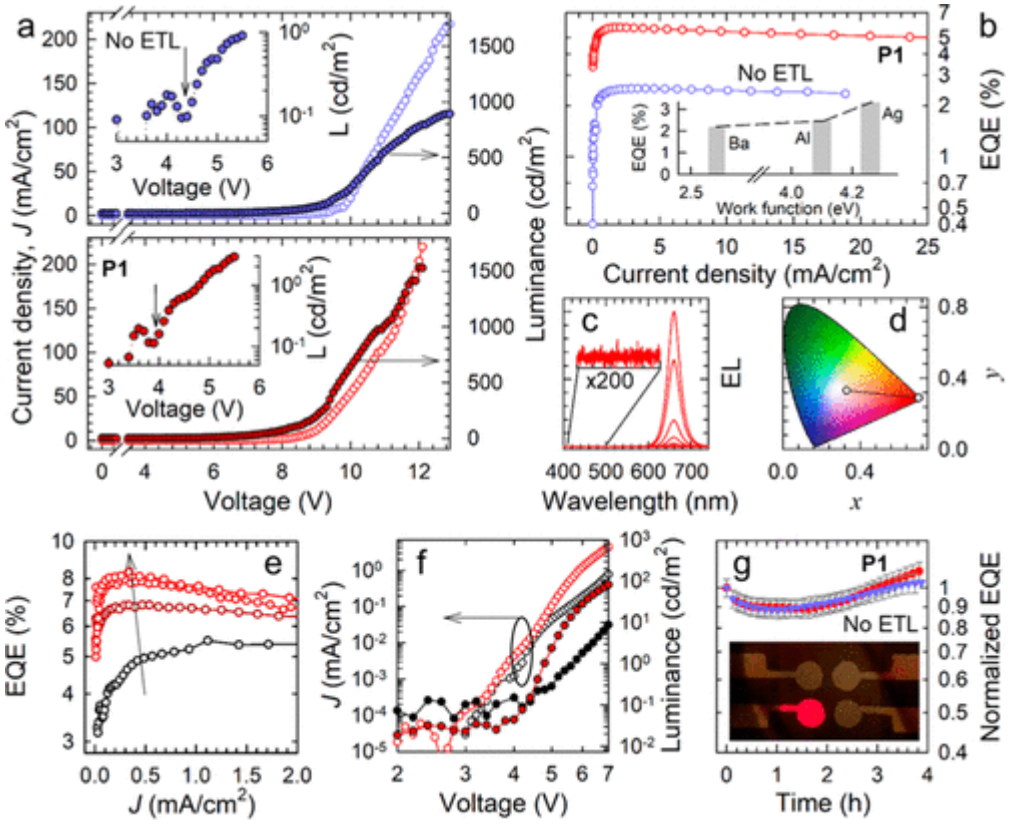

Figure 3. (a) Current-density–voltage–luminance (J–V–L) responses of solution-processed NPL-LEDs containing CdSe/CdZnS NPLs without the polar polymer ETL (blue symbols) and with P1 ETL (red symbols). The complete device structures are ITO/PEDOT:PSS/PVK/NPLs/Al and ITO/PEDOT:PSS/PVK/NPLs/P1/Al, respectively. Inset: magnification of the low-voltage portion (3–6 V, semi-logarithmic scale) of the V–L plot, with arrows pointing to the turn-on voltages. (b) EQE for the devices in panel a as a function of J. Inset: maximum EQE for LEDs without ETL as a function of the work function of the metal cathode. (c) Electroluminescence (EL) spectra of the NPL-LED with P1 ETL at increasing driving voltage from 4 to 11 V. Inset: enlargement of the EL at 11 V between 400 and 500 nm, highlighting the absence of EL contributions by the polymeric interlayers. (d) Chromaticity coordinates for the EL reported in panel c, projected onto the

CIE chromaticity diagram, highlighting the vicinity of the color coordinates to the spectral locus. Saturation is 98%. (e) EQE for the NPL-LED with P1 ETL as a function of J, recorded for the pristine device in nitrogen atmosphere (black circles) and after exposure to atmospheric conditions for 15, 30, and 330 min as indicated by the arrow. (f) J–V–L responses of NPL-LEDs with P1 ETL, recorded for the pristine device in nitrogen (black symbols) and after 330 min of exposure to atmospheric conditions (red symbols). (g) Normalized EQE for NPL-LEDs with and without P1 ETL (red and blue dots, respectively; error bars are displayed in gray) monitored over 4 h of continuous operation in humid (50%) air. Prior to the measurement, the LEDs were stored in air for 5 h to saturate the efficiency enhancement effect shown in panel e. Inset: photograph of a working LED with P1 interlayer and Al cathode. Bright emission is observed over the whole device area (5.4 mm2) under a driving bias of 6 V.

Table 1. External Quantum Efficiency (EQE, Percent) of ITO/PEDOT:PSS/PVK/(CdSe/CdZnS) NPLs/ETL/Metal Cathode LEDs With and Without a P1 ETL and Featuring Different Metal Cathodes. The best result for each device structure is reported in bold. a

metal cathode	work function, Φ (eV)	CPE ETL	as fabricated in N_2, <EQE> ± SD/best	after air exposure (>50% humidity), <EQE> ± SD/best
Ba/Al	2.52−2.7	no	2.15 ± 0.03/**2.17**	2.5 ± 0.30/**2.56**
		P1	3.48 ± 0.13/**3.60**	7.60 ± 0.5/**7.74**
Al	4.06−4.26	no	2.43 ± 0.07/**2.47**	4.2 ± 0.2/**4.36**
		P1	5.61 ± 0.17/**5.73**	8.0 ± 0.4/**8.39**
Ag	4.26−4.74	no	2.80 ± 0.40/**3.31**	3.57 ± 0.19/**3.76**
		P1	4.98 ± 0.19/**5.11**	6.20 ± 0.50/**6.59**

[a]The EQE values after exposure in air for 30 min are also reported.

A closer look at the EQE curves in Figure 3b reveals a very weak roll-off with increasing current density, which is in agreement with the behavior of LEDs containing CdSe/CdS hetero-QDs and homopolymeric CPE interlayers. (35) The EL spectra as a function of the driving voltage for the NPL-LEDs with P1 are reported in Figure 3c (see Figure S5 for the LED without P1), showing a symmetric EL peak centered at 658 nm (full width at half-maximum = 25 nm). No spurious emission from the polymeric interlayers is observed (see the inset of Figure 3c), which confirms that exciton recombination occurs exclusively inside the NPL active layer. The corresponding CIE (Commision International de l'Eclairage) color coordinates are x = 0.71 and y = 0.29, corresponding to 98% saturated deep-red light ideal for wide-gamut RGB displays (Figure 2d). This result, together with a >1500 cd/m2 luminance for the polymer-embedding device, further endorses the strength of our approach for lighting applications, especially if we take into account that such brightness occurs in a spectral region where the human eye sensitivity is less than 10% in photopic conditions (10–108 cd/m2).

As anticipated, exposure of the NPL-LEDs to air dramatically enhances their efficiency, leading to EQEs as high as 8.4% for the LED containing the P1 ETL and the Al cathode (the values for the whole set of LEDs is summarized in Table 1), which exceeds the best reports of red NPL-LEDs by over 1 order of magnitude and sets a new global record for QD-LEDs of any color containing all solution-based organic interlayers (see Table S1). (32) This result is particularly relevant if one takes into account that the NPL employed for this study were not optimized for their emission efficiency (ΦPL = 40 ± 5%). This indicates that, by using optimized NPLs with ΦPL > 95% in combination with our device architecture, EQEs as high as 20% could be achieved, which corresponds to the external efficiency of “ideal” planar LEDs with no engineered light out-coupling. (33,34) Our results thus strongly suggest that the internal efficiency as high as 100% obtained

with spherical QDs (33,34) can also be achieved with two-dimensional colloidal nanostructures. To experimentally illustrate the beneficial effect of air on our LEDs, we measured the EQE upon extended exposure to air without any encapsulation. Figure 3e reports the EQE as a function of the current density for an NPL-LED containing P1 and an Al cathode under nitrogen atmosphere and after 15, 30, and 330 min in environmental air. The EQE displays a remarkable improvement after exposure to ambient air, reaching 8.4% after 5 h with very limited efficiency roll-off. We notice that this effect occurs with minimal variation of the current density and is mostly due to increased brightness (Figure 3f) in air. However, PL measurements in vacuum, in pure O2, and in humid air reveal that the emission efficiency of the NPLs is essentially unaffected by the external atmosphere (only 5% higher in vacuum, which is close to the experimental resolution; see Figures S6–9). (27) The PL decay traces measured under device operation below and above VON further indicate that ΦPL is unaffected by the electric field and current density (Figure S10). We therefore identify the partial oxidation of the metal cathode as a possible cause of the enhanced EQE in air, leading to a nearly optimal charge balance due to the slightly increased electrode work function without measurable reductions of the current density. In support of this interpretation, we measured the contact potential difference between tip and surface of bare and modified (P1-covered) Al thin films on glass by the Kelvin-probe technique. The measurements under nitrogen atmosphere show the ability of P1 to reduce the metal work function (|WF|) as a result of the formation of the interface dipole. Exposure to humid air (50%), however, increases |WF| of both bare and covered Al film, in agreement with partial oxidation effects (Figure S11).

Most importantly for the practical application of NPLs in LEDs, our devices exhibit exceptional stability in environmental air for many hours of continuous operation. The EQE versus time traces in Figure 3g (for an NPL-LED stored in air for 5 h) clearly indicate that, after an initial assessment period of around 1 h of operation, which sees a ∼10% efficiency reduction, the EQE fully recovers and reaches a further ∼10% increase over the initial value after 4 h of continuous drive in air. This is unexpected because in conventional LEDs, the use of Al is a stability-limiting factor. Upon exposure to water or oxygen, Al cathodes rapidly oxidize to insulating aluminum oxide, (88) and the growth of a barrier to electron injection is usually detrimental for the device performance. It is, however, worth noticing that the insertion of a buffer layer of Al2O3 between the Al cathode and the active layer in some organic LEDs has been observed to increase the device efficiency, which was ascribed to enhanced carrier density near the metal/organic interface. (89,90) In our case, as discussed above, the partial oxidation of the Al electrode does not completely inhibit charge injection but further regulates the electron concentration in the active layer, leading to enhanced charge balance and higher EQE.

Conclusions

In conclusion, by combining narrow-band-emitting NPLs with a multifunctional polar and electrolytic polymer expressly designed as ETL material, we have created high-efficiency NPL-LEDs with saturated red EL using exclusively solution-based methods. As a result of the improved charge balance provided by the ETL, our proof-of-concept NPL-LEDs function close to ideal devices, with the emission efficiency of the active layer being the only limiting factor to the EQE and exceeding the previous reports of red-emitting NPL-LEDs by 1 order of magnitude. Exposure to humid air strongly enhances the performances of our devices and leads to the record value of EQE = 8.39%, which is further found to be stable under continuous operation in air for many hours without encapsulation. Our results clearly demonstrate the potential of two-dimensional colloidal nanostructures for color-saturated, efficient, and reliable displays. (91−93)

Author Information

Corresponding Authors

Umberto Giovanella - Istituto per lo Studio delle Macromolecole, Consiglio Nazionale delle Ricerche (ISMac-CNR), Via Bassini 15, 20133 Milano, Italy; Email: u.giovanella@ismac.cnr.it

Benoit Dubertret - Laboratoire de Physique et d'Etude des Matériaux, ESPCI-ParisTech, PSL Research University, Sorbonne Université UPMC Université Paris 06, CNRS, 10 rue Vauquelin, 75005 Paris, France; Email: benoit.dubertret@espci.fr

Sergio Brovelli - Dipartimento di Scienza dei Materiali, Università degli Studi di Milano-Bicocca, via Cozzi 55, I-20125 Milano, Italy; Orcidhttp://orcid.org/0000-0002-5993-855X; Email: sergio.brovelli@unimib.it

Authors

Mariacecilia Pasini - Istituto per lo Studio delle Macromolecole, Consiglio Nazionale delle Ricerche (ISMac-CNR), Via Bassini 15, 20133 Milano, Italy

Monica Lorenzon - Dipartimento di Scienza dei Materiali, Università degli Studi di Milano-Bicocca, via Cozzi 55, I-20125 Milano, Italy; Orcidhttp://orcid.org/0000-0003-3524-9546

Francesco Galeotti - Istituto per lo Studio delle Macromolecole, Consiglio Nazionale delle Ricerche (ISMac-CNR), Via Bassini 15, 20133 Milano, Italy; Orcidhttp://orcid.org/0000-0003-4793-9827

Claudio Lucchi - Dipartimento di Scienza dei Materiali, Università degli Studi di Milano-Bicocca, via Cozzi 55, I-20125 Milano, Italy

Francesco Meinardi - Dipartimento di Scienza dei Materiali, Università degli Studi di Milano-Bicocca, via Cozzi 55, I-20125 Milano, Italy

Silvia Luzzati - Istituto per lo Studio delle Macromolecole, Consiglio Nazionale delle Ricerche (ISMac-CNR), Via Bassini 15, 20133 Milano, Italy

Notes

The authors declare no competing financial interest.

Acknowledgments

The authors thank Nexdot (http://www.nexdot.fr) for providing samples. M.L. thanks the Fondazione Cassa di Risparmio di Tortona for financial support. U.G, M.P, F.G, and S.L. thank the ACCORDO QUADRO Regione Lombardia project (7784/2016) "I-ZEB" for financial support. Lorenzo Meazza (ISMAC–CNR) is acknowledged for assistance with the synthesis of conjugated monomers. Authors thank Dr. Guido Scavia (ISMAC-CNR) for Kelvin-probe measurements. This work is dedicated to the loving memory of Gianluca Latini, friend and colleague.

References

1Ithurria, S.; Dubertret, B. J. Am. Chem. Soc. 2008, 130, 16504– 16505, DOI: 10.1021/ja807724e [ACS Full Text ACS Full Text], [CAS], Google Scholar

2Ithurria, S.; Bousquet, G.; Dubertret, B. J. Am. Chem. Soc. 2011, 133, 3070– 3077, DOI: 10.1021/ja110046d [ACS Full Text ACS Full Text], Google Scholar

3Ithurria, S.; Tessier, M. D.; Mahler, B.; Lobo, R. P. S. M.; Dubertret, B.; Efros, A. L. Nat. Mater. 2011, 10, 936– 941, DOI: 10.1038/nmat3145 [Crossref], [PubMed], [CAS], Google Scholar

4Ithurria, S.; Talapin, D. V. J. Am. Chem. Soc. 2012, 134, 18585– 18590, DOI: 10.1021/ja308088d [ACS Full Text ACS Full Text], [CAS], Google Scholar

5Bouet, C.; Mahler, B.; Nadal, B.; Abecassis, B.; Tessier, M. D.; Ithurria, S.; Xu, X.; Dubertret, B. Chem. Mater. 2013, 25, 639– 645, DOI: 10.1021/cm304080q [ACS Full Text ACS Full Text], Google Scholar

6Bouet, C.; Tessier, M. D.; Ithurria, S.; Mahler, B.; Nadal, B.; Dubertret, B. Chem. Mater. 2013, 25, 1262– 1271, DOI: 10.1021/cm303786a [ACS Full Text ACS Full Text], Google Scholar

7Khan, A. H.; Brescia, R.; Polovitsyn, A.; Angeloni, I.; Martín-García, B.; Moreels, I. Chem. Mater. 2017, 29, 2883– 2889, DOI: 10.1021/acs.chemmater.6b05111 [ACS Full Text ACS Full Text], Google Scholar

8Pelton, M.; Ithurria, S.; Schaller, R. D.; Dolzhnikov, D. S.; Talapin, D. V. Nano Lett. 2012, 12, 6158– 6163, DOI: 10.1021/nl302986y [ACS Full Text ACS Full Text], Google Scholar

9Scholes, G. D. Nat. Mater. 2011, 10, 906– 907, DOI: 10.1038/nmat3183 [Crossref], Google Scholar

10She, C.; Fedin, I.; Dolzhnikov, D. S.; Demortière, A.; Schaller, R. D.; Pelton, M.; Talapin, D. V. Nano Lett. 2014, 14, 2772– 2777, DOI: 10.1021/nl500775p [ACS Full Text ACS Full Text], [CAS], Google Scholar

11Achtstein, A. W.; Schliwa, A.; Prudnikau, A.; Hardzei, M.; Artemyev, M. V.; Thomsen, C.; Woggon, U. Nano Lett. 2012, 12, 3151– 3157, DOI: 10.1021/nl301071n [ACS Full Text ACS Full Text], [CAS], Google Scholar

12Zhang, F.; Wang, S.; Wang, L.; Lin, Q.; Shen, H.; Cao, W.; Yang, C.; Wang, H.; Yu, L.; Du, Z.; Xue, J.; Li, L. S. Nanoscale 2016, 8, 12182– 12188, DOI: 10.1039/C6NR02922A [Crossref], Google Scholar

13Tessier, M. D.; Biadala, L.; Bouet, C.; Ithurria, S.; Abecassis, B.; Dubertret, B. ACS Nano 2013, 7, 3332– 3340, DOI: 10.1021/nn400833d [ACS Full Text ACS Full Text], Google Scholar

14Riedinger, A.; Ott, F. D.; Mule, A.; Mazzotti, S.; Knüsel, P. N.; Kress, S. J. P.; Prins, F.; Erwin, S. C.; Norris, D. J. Nat. Mater. 2017, DOI: 10.1038/nmat4889 [Crossref], Google Scholar

15Tessier, M. D.; Mahler, B.; Nadal, B.; Heuclin, H.; Pedetti, S.; Dubertret, B. Nano Lett. 2013, 13, 3321– 3328, DOI: 10.1021/nl401538n [ACS Full Text ACS Full Text], Google Scholar

16Naeem, A.; Masia, F.; Christodoulou, S.; Moreels, I.; Borri, P.; Langbein, W. Phys. Rev. B: Condens. Matter Mater. Phys. 2015, 91, 121302, DOI: 10.1103/PhysRevB.91.121302 [Crossref], [CAS], Google Scholar

17Grim, J. Q.; Christodoulou, S.; Di Stasio, F.; Krahne, R.; Cingolani, R.; Manna, L.; Moreels, I. Nat. Nanotechnol. 2014, 9, 891, DOI: 10.1038/nnano.2014.213 [Crossref], [PubMed], [CAS], Google Scholar

18Kunneman, L. T.; Schins, J. M.; Pedetti, S.; Heuclin, H.; Grozema, F. C.; Houtepen, A. J.; Dubertret, B.; Siebbeles, L. D. A. Nano Lett. 2014, 14, 7039– 7045, DOI: 10.1021/nl503406a [ACS Full Text ACS Full Text], Google Scholar

19Kunneman, L. T.; Tessier, M. D.; Heuclin, H.; Dubertret, B.; Aulin, Y. V.; Grozema, F. C.; Schins, J. M.; Siebbeles, L. D. A. J. Phys. Chem. Lett. 2013, 4, 3574– 3578, DOI: 10.1021/jz401970p [ACS Full Text ACS Full Text], [CAS], Google Scholar

20Li, M.; Zhi, M.; Zhu, H.; Wu, W.-Y.; Xu, Q.-H.; Jhon, M. H.; Chan, Y. Nat. Commun. 2015, 6.Google Scholar

21Guzelturk, B.; Kelestemur, Y.; Olutas, M.; Delikanli, S.; Demir, H. V. ACS Nano 2014, 8, 6599– 6605, DOI: 10.1021/nn5022296 [ACS Full Text ACS Full Text], [CAS], Google Scholar

22Lhuillier, E.; Dayen, J.-F.; Thomas, D. O.; Robin, A.; Doudin, B.; Dubertret, B. Nano Lett. 2015, 15, 1736, DOI: 10.1021/nl504414g [ACS Full Text ACS Full Text], Google Scholar

23Bi, W.; Zhou, M.; Ma, Z.; Zhang, H.; Yu, J.; Xie, Y. Chem. Commun. 2012, 48, 9162– 9164, DOI: 10.1039/c2cc34727j [Crossref], Google Scholar

24Lhuillier, E.; Robin, A.; Ithurria, S.; Aubin, H.; Dubertret, B. Nano Lett. 2014, 14, 2715– 2719, DOI: 10.1021/nl5006383 [ACS Full Text ACS Full Text], [CAS], Google Scholar

25Lhuillier, E.; Ithurria, S.; Descamps-Mandine, A.; Douillard, T.; Castaing, R.; Xu, X. Z.; Taberna, P.-L.; Simon, P.; Aubin, H.; Dubertret, B. J. Phys. Chem. C 2015, 119, 21795– 21799, DOI: 10.1021/acs.jpcc.5b05296 [ACS Full Text ACS Full Text], [CAS], Google Scholar

26Lhuillier, E.; Pedetti, S.; Ithurria, S.; Heuclin, H.; Nadal, B.; Robin, A.; Patriarche, G.; Lequeux, N.; Dubertret, B. ACS Nano 2014, 8, 3813– 3820, DOI: 10.1021/nn500538n [ACS Full Text ACS Full Text], Google Scholar

27Lorenzon, M.; Christodoulou, S.; Vaccaro, G.; Pedrini, J.; Meinardi, F.; Moreels, I.; Brovelli, S. Nat. Commun. 2015, 6.[Crossref], [PubMed], Google Scholar

28Chen, Z.; Nadal, B.; Mahler, B.; Aubin, H.; Dubertret, B. Adv. Funct. Mater. 2014, 24, 295– 302, DOI: 10.1002/adfm.201301711 [Crossref], [CAS], Google Scholar

29Fan, F.; Kanjanaboos, P.; Saravanapavanantham, M.; Beauregard, E.; Ingram, G.; Yassitepe, E.; Adachi, M. M.; Voznyy, O.; Johnston, A. K.; Walters, G.; Kim, G.-H.; Lu, Z.-H.; Sargent, E. H. Nano Lett. 2015, 15, 4611, DOI: 10.1021/acs.nanolett.5b01233 [ACS Full Text ACS Full Text], [CAS], Google Scholar

30Vitukhnovsky, A. G.; Lebedev, V. S.; Selyukov, A. S.; Vashchenko, A. A.; Vasiliev, R. B.; Sokolikova, M. S. Chem. Phys. Lett. 2015, 619, 185– 188, DOI: 10.1016/j.cplett.2014.12.002 [Crossref], [CAS], Google Scholar

31Ott, F. D.; Riedinger, A.; Ochsenbein, D. R.; Knüsel, P. N.; Erwin, S. C.; Mazzotti, M.; Norris, D. J. Nano Lett. 2017, 17, 6870, DOI: 10.1021/acs.nanolett.7b03191 [ACS Full Text ACS Full Text], [CAS], Google Scholar

32Pietryga, J. M.; Park, Y.-S.; Lim, J.; Fidler, A. F.; Bae, W. K.; Brovelli, S.; Klimov, V. I. Chem. Rev. 2016, 116, 10513– 10622, DOI: 10.1021/acs.chemrev.6b00169 [ACS Full Text ACS Full Text], [CAS], Google Scholar

33Dai, X.; Zhang, Z.; Jin, Y.; Niu, Y.; Cao, H.; Liang, X.; Chen, L.; Wang, J.; Peng, X. Nature 2014, 515, 96– 99, DOI: 10.1038/nature13829 [Crossref], [PubMed], [CAS], Google Scholar

34Mashford, B. S.; Stevenson, M.; Popovic, Z.; Hamilton, C.; Zhou, Z.; Breen, C.; Steckel, J.; Bulovic, V.; Bawendi, M.; Coe-Sullivan, S.; Kazlas, P. T. Nat. Photonics 2013, 7, 407– 412, DOI: 10.1038/nphoton.2013.70 [Crossref], [CAS], Google Scholar

35Castelli, A.; Meinardi, F.; Pasini, M.; Galeotti, F.; Pinchetti, V.; Lorenzon, M.; Manna, L.; Moreels, I.; Giovanella, U.; Brovelli, S. Nano Lett. 2015, 15, 5455– 5464, DOI: 10.1021/acs.nanolett.5b01849 [ACS Full Text ACS Full Text], Google Scholar

36Huang, F.; Wu, H.; Cao, Y. Chem. Soc. Rev. 2010, 39, 2500– 2521, DOI: 10.1039/b907991m [Crossref], Google Scholar

37Huang, F.; Wu, H.; Peng, J.; Yang, W.; Cao, Y. Curr. Org. Chem. 2007, 11, 1207– 1219, DOI: 10.2174/138527207781696017 [Crossref], [CAS], Google Scholar

38Huang, F.; Wu, H.; Wang, D.; Yang, W.; Cao, Y. Chem. Mater. 2004, 16, 708– 716, DOI: 10.1021/cm034650o [ACS Full Text ACS Full Text], Google Scholar

39Liu, C.; Tan, Y.; Li, C.; Wu, F.; Chen, L.; Chen, Y. ACS Appl. Mater. Interfaces 2015, 7, 19024– 19033, DOI: 10.1021/acsami.5b03340 [ACS Full Text ACS Full Text], Google Scholar

40Duan, C.; Wang, L.; Zhang, K.; Guan, X.; Huang, F. Adv. Mater. 2011, 23, 1665– 1669, DOI: 10.1002/adma.201004661 [Crossref], Google Scholar

41Duarte, A.; Pu, K.-Y.; Liu, B.; Bazan, G. C. Chem. Mater. 2011, 23, 501– 515, DOI: 10.1021/cm102196t [ACS Full Text ACS Full Text], Google Scholar

42Pinto, M. R.; Schanze, K. S. Synthesis 2002, 2002, 1293– 1309, DOI: 10.1055/s-2002-32541 [Crossref], Google Scholar

43Lee, B. H.; Jung, I. H.; Woo, H. Y.; Shim, H.-K.; Kim, G.; Lee, K. Adv. Funct. Mater. 2014, 24, 1100– 1108, DOI: 10.1002/adfm.201301810 [Crossref], Google Scholar

44Hoven, C. V.; Garcia, A.; Bazan, G. C.; Nguyen, T.-Q. Adv. Mater. 2008, 20, 3793– 3810, DOI: 10.1002/adma.200800533 [Crossref], Google Scholar

45Ahn, J.-H.; Kim, H.-S.; Lee, K. J.; Jeon, S.; Kang, S. J.; Sun, Y.; Nuzzo, R. G.; Rogers, J. A. Science 2006, 314, 1754– 1757, DOI: 10.1126/science.1132394 [Crossref], Google Scholar

46Cho, K.-S.; Lee, E. K.; Joo, W.-J.; Jang, E.; Kim, T.-H.; Lee, S. J.; Kwon, S.-J.; Han, J. Y.; Kim, B.-K.; Choi, B. L.; Kim, J. M. Nat. Photonics 2009, 3, 341– 345, DOI: 10.1038/nphoton.2009.92 [Crossref], [CAS], Google Scholar

47Kim, L.; Anikeeva, P. O.; Coe-Sullivan, S. A.; Steckel, J. S.; Bawendi, M. G.; Bulović, V. Nano Lett. 2008, 8, 4513– 4517, DOI: 10.1021/nl8025218 [ACS Full Text ACS Full Text], Google Scholar

48Kim, T.-H.; Cho, K.-S.; Lee, E. K.; Lee, S. J.; Chae, J.; Kim, J. W.; Kim, D. H.; Kwon, J.-Y.; Amaratunga, G.; Lee, S. Y.; Choi, B. L.; Kuk, Y.; Kim, J. M.; Kim, K. Nat. Photonics 2011, 5, 176– 182, DOI: 10.1038/nphoton.2011.12 [Crossref], [CAS], Google Scholar

49Kim, T.-H.; Chung, D.-Y.; Ku, J.; Song, I.; Sul, S.; Kim, D.-H.; Cho, K.-S.; Choi, B. L.; Kim, J. M.; Hwang, S.; Min Kim, J. Nat. Commun. 2013, 4, 2637, DOI: 10.1038/ncomms3637 [Crossref], [PubMed], [CAS], Google Scholar

50Latini, G.; Winroth, G.; Brovelli, S.; McDonnell, S. O.; Anderson, H. L.; Mativetsky, J. M.; Samori, P.; Cacialli, F. J. Appl. Phys. 2010, 107, 124509[Crossref], [CAS], Google Scholar

51Latini, G.; Parrott, L. J.; Brovelli, S.; Frampton, M. J.; Anderson, H. L.; Cacialli, F. Adv. Funct. Mater. 2008, 18, 2419– 2427, DOI: 10.1002/adfm.200800120 [Crossref], Google Scholar

52Hoven, C. V.; Yang, R.; Garcia, A.; Crockett, V.; Heeger, A. J.; Bazan, G. C.; Nguyen, T.-Q. Proc. Natl. Acad. Sci. U. S. A. 2008, 105, 12730– 12735, DOI: 10.1073/pnas.0806494105 [Crossref], Google Scholar

53Zinna, F.; Pasini, M.; Galeotti, F.; Botta, C.; Di Bari, L.; Giovanella, U. Adv. Funct. Mater. 2017, 27, 1603719, DOI: 10.1002/adfm.201603719 [Crossref], Google Scholar

54Seo, J. H.; Gutacker, A.; Sun, Y.; Wu, H.; Huang, F.; Cao, Y.; Scherf, U.; Heeger, A. J.; Bazan, G. C. J. Am. Chem. Soc. 2011, 133, 8416– 8419, DOI: 10.1021/ja2037673 [ACS Full Text ACS Full Text], Google Scholar

55Yang, T.; Wang, M.; Duan, C.; Hu, X.; Huang, L.; Peng, J.; Huang, F.; Gong, X. Energy Environ. Sci. 2012, 5, 8208– 8214, DOI: 10.1039/c2ee22296e [Crossref], Google Scholar

56Hikmet, R. A. M.; Chin, P. T. K.; Talapin, D. V.; Weller, H. Adv. Mater. 2005, 17, 1436– 1439, DOI: 10.1002/adma.200401763 [Crossref], Google Scholar

57Son, D. I.; Kim, H. H.; Cho, S.; Hwang, D. K.; Seo, J. W.; Choi, W. K. Org. Electron. 2014, 15, 886– 892, DOI: 10.1016/j.orgel.2014.01.014 [Crossref], [CAS], Google Scholar

58Son, D. I.; Kim, H. H.; Hwang, D. K.; Kwon, S.; Choi, W. K. J. Mater. Chem. C 2014, 2, 510– 514, DOI: 10.1039/C3TC31297F [Crossref], [CAS], Google Scholar

59Zhao, L.; Zhou, Z.-L.; Guo, Z.; Pei, J.; Mao, S. MRS Online Proc. Libr. 2011, 1359, 1359, DOI: 10.1557/opl.2011.884 [Crossref], Google Scholar

60Bae, W. K.; Lim, J.; Zorn, M.; Kwak, J.; Park, Y.-S.; Lee, D.; Lee, S.; Char, K.; Zentel, R.; Lee, C. J. Mater. Chem. C 2014, 2, 4974– 4979, DOI: 10.1039/C4TC00232F [Crossref], [CAS], Google Scholar

61Ippen, C.; Greco, T.; Kim, Y.; Kim, J.; Oh, M. S.; Han, C. J.; Wedel, A. Org. Electron. 2014, 15, 126– 131, DOI: 10.1016/j.orgel.2013.11.003 [Crossref], [CAS], Google Scholar

62Zhang, Y.; Xie, C.; Su, H.; Liu, J.; Pickering, S.; Wang, Y.; Yu, W. W.; Wang, J.; Wang, Y.; Hahm, J.-i.; Dellas, N.; Mohney, S. E.; Xu, J. Nano Lett. 2011, 11, 329– 332, DOI: 10.1021/nl1021442 [ACS Full Text ACS Full Text], Google Scholar

63Cho, I.; Jung, H.; Jeong, B. G.; Chang, J. H.; Kim, Y.; Char, K.; Lee, D. C.; Lee, C.; Cho, J.; Bae, W. K. ACS Nano 2017, 11, 684– 692, DOI: 10.1021/acsnano.6b07028 [ACS Full Text ACS Full Text], Google Scholar

64Huang, J.; Xu, Z.; Yang, Y. Adv. Funct. Mater. 2007, 17, 1966– 1973, DOI: 10.1002/adfm.200700051 [Crossref], Google Scholar

65Zhang, B.; Qin, C.; Niu, X.; Xie, Z.; Cheng, Y.; Wang, L.; Li, X. Appl. Phys. Lett. 2010, 97, 043506, DOI: 10.1063/1.3475021 [Crossref], Google Scholar

66Brütting, W.; Frischeisen, J.; Schmidt, T. D.; Scholz, B. J.; Mayr, C. Phys. Status Solidi A 2013, 210, 44– 65, DOI: 10.1002/pssa.201228320 [Crossref], Google Scholar

67Nam, S.; Oh, N.; Zhai, Y.; Shim, M. ACS Nano 2015, 9, 878– 885, DOI: 10.1021/nn506577p [ACS Full Text ACS Full Text], Google Scholar

68Cho, N. S.; Hwang, D.-H.; Lee, J.-I.; Jung, B.-J.; Shim, H.-K. Macromolecules 2002, 35, 1224– 1228, DOI: 10.1021/ma011155+ [ACS Full Text ACS Full Text], Google Scholar

69Frampton, M. J.; Sforazzini, G.; Brovelli, S.; Latini, G.; Townsend, E.; Williams, C. C.; Charas, A.; Zalewski, L.; Kaka, N. S.; Sirish, M.; Parrott, L. J.; Wilson, J. S.; Cacialli, F.; Anderson, H. L. Adv. Funct. Mater. 2008, 18, 3367– 3376, DOI: 10.1002/adfm.200800653 [Crossref], Google Scholar

70Seo, J. H.; Yang, R.; Brzezinski, J. Z.; Walker, B.; Bazan, G. C.; Nguyen, T.-Q. Adv. Mater. 2009, 21, 1006– 1011, DOI: 10.1002/adma.200802420 [Crossref], Google Scholar

71Liu, B.; Bazan, G. C. Conjugated polyelectrolytes: fundamentals and applications; John Wiley & Sons: Hoboken, NJ, 2013.Google Scholar

72Yap, B. K.; Xia, R.; Campoy-Quiles, M.; Stavrinou, P. N.; Bradley, D. D. C. Nat. Mater. 2008, 7, 376– 380, DOI: 10.1038/nmat2165 [Crossref], Google Scholar

73Rowland, C. E.; Fedin, I.; Zhang, H.; Gray, S. K.; Govorov, A. O.; Talapin, D. V.; Schaller, R. D. Nat. Mater. 2015, 14, 484[Crossref], [PubMed], [CAS], Google Scholar

74Guzelturk, B.; Erdem, O.; Olutas, M.; Kelestemur, Y.; Demir, H. V. ACS Nano 2014, 8, 12524– 12533, DOI: 10.1021/nn5053734 [ACS Full Text ACS Full Text], [CAS], Google Scholar

75Abécassis, B.; Tessier, M. D.; Davidson, P.; Dubertret, B. Nano Lett. 2014, 14, 710– 715, DOI: 10.1021/nl4039746 [ACS Full Text ACS Full Text], Google Scholar

76Erdem, O.; Olutas, M.; Guzelturk, B.; Kelestemur, Y.; Demir, H. V. J. Phys. Chem. Lett. 2016, 7, 548– 554, DOI: 10.1021/acs.jpclett.5b02763 [ACS Full Text ACS Full Text], [CAS], Google Scholar

77Rowland, C. E.; Fedin, I.; Zhang, H.; Gray, S. K.; Govorov, A. O.; Talapin, D. V.; Schaller, R. D. Nat. Mater. 2015, 14, 484, DOI: 10.1038/nmat4231 [Crossref], [PubMed], [CAS], Google Scholar

78Guzelturk, B.; Olutas, M.; Delikanli, S.; Kelestemur, Y.; Erdem, O.; Demir, H. V. Nanoscale 2015, 7, 2545– 2551, DOI: 10.1039/C4NR06003B [Crossref], [PubMed], [CAS], Google Scholar

79Olutas, M.; Guzelturk, B.; Kelestemur, Y.; Gungor, K.; Demir, H. V. Adv. Funct. Mater. 2016, 26, 2891– 2899, DOI: 10.1002/adfm.201505108 [Crossref], Google Scholar

80Pal, B. N.; Ghosh, Y.; Brovelli, S.; Laocharoensuk, R.; Klimov, V. I.; Hollingsworth, J. A.; Htoon, H. Nano Lett. 2012, 12, 331– 336, DOI: 10.1021/nl203620f [ACS Full Text ACS Full Text], [CAS], Google Scholar

81Bae, W. K.; Park, Y.-S.; Lim, J.; Lee, D.; Padilha, L. A.; McDaniel, H.; Robel, I.; Lee, C.; Pietryga, J. M.; Klimov, V. I. Nat. Commun. 2013, 4, 2661, DOI: 10.1038/ncomms3661 [Crossref], [PubMed], [CAS], Google Scholar

82Brovelli, S.; Bae, W. K.; Galland, C.; Giovanella, U.; Meinardi, F.; Klimov, V. I. Nano Lett. 2014, 14, 486– 494, DOI: 10.1021/nl403478s [ACS Full Text ACS Full Text], Google Scholar

83Bae, W. K.; Klimov, V. I.; Brovelli, S. MRS Bull. 2013, 38, 721– 730, DOI: 10.1557/mrs.2013.182 [Crossref], Google Scholar

84Bozyigit, D.; Yarema, O.; Wood, V. Adv. Funct. Mater. 2013, 23, 3024– 3029, DOI: 10.1002/adfm.201203191 [Crossref], Google Scholar

85Hoven, C.; Yang, R.; Garcia, A.; Heeger, A. J.; Nguyen, T.-Q.; Bazan, G. C. J. Am. Chem. Soc. 2007, 129, 10976– 10977, DOI: 10.1021/ja072612q [ACS Full Text ACS Full Text], Google Scholar

86Jin, Y.; Bazan, G. C.; Heeger, A. J.; Kim, J. Y.; Lee, K. Appl. Phys. Lett. 2008, 93, 123304, DOI: 10.1063/1.2989133 [Crossref], Google Scholar

87Yang, R.; Xu, Y.; Dang, X.-D.; Nguyen, T.-Q.; Cao, Y.; Bazan, G. C. J. Am. Chem. Soc. 2008, 130, 3282– 3283, DOI: 10.1021/ja711068d [ACS Full Text ACS Full Text], Google Scholar

88Krebs, F. C.; Norrman, K. Prog. Photovoltaics 2007, 15, 697– 712, DOI: 10.1002/pip.794 [Crossref], Google Scholar

89Li, F.; Tang, H.; Anderegg, J.; Shinar, J. Appl. Phys. Lett. 1997, 70, 1233– 1235, DOI: 10.1063/1.118539 [Crossref], Google Scholar

90Zhang, S. T.; Zhou, Y. C.; Zhao, J. M.; Zhan, Y. Q.; Wang, Z. J.; Wu, Y.; Ding, X. M.; Hou, X. Y. Appl. Phys. Lett. 2006, 89, 043502, DOI: 10.1063/1.2220013 [Crossref], Google Scholar

91Liu, B.; Dishari, S. K. Chem. - Eur. J. 2008, 14, 7366– 7375, DOI: 10.1002/chem.200701906 [Crossref], [PubMed], [CAS], Google Scholar

92Zhou, G.; Qian, G.; Ma, L.; Cheng, Y.; Xie, Z.; Wang, L.; Jing, X.; Wang, F. Macromolecules 2005, 38, 5416– 5424, DOI: 10.1021/ma050807h [ACS Full Text ACS Full Text], Google Scholar

93Mahler, B.; Spinicelli, P.; Buil, S.; Quelin, X.; Hermier, J.-P.; Dubertret, B. Nat. Mater. 2008, 7, 659– 664, DOI: 10.1038/nmat2222 [Crossref], Google Scholar